Phys Chem Minerals (2013) 40:195–201
DOI 10.1007/s00269-012-0558-0

ORIGINAL PAPER

Sound velocities of $Na_{0.4}Mg_{0.6}Al_{1.6}Si_{0.4}O_4$ NAL and CF phases to 73 GPa determined by Brillouin scattering method

Lidong Dai · Yuki Kudo · Kei Hirose · Motohiko Murakami · Yuki Asahara · Haruka Ozawa · Yasuo Ohishi · Naohisa Hirao

Received: 6 September 2012 / Accepted: 7 December 2012 / Published online: 9 February 2013

Abstract The sound velocities of two aluminum-rich phases in the lower mantle, hexagonal new Al-rich phase (NAL) and its corresponding high-pressure polymorph orthorhombic Ca-ferrite-type phase (CF), were determined with the Brillouin scattering method in a pressure range from 9 to 73 GPa at room temperature. Both NAL and CF samples have identical chemical composition of $Na_{0.4}Mg_{0.6}Al_{1.6}Si_{0.4}O_4$ (40 % $NaAlSiO_4$–60 % $MgAl_2O_4$). Infrared laser annealing in the diamond anvil cell was performed to minimize the stress state of the sample and obtain the high-quality Brillouin spectra. The results show shear modulus at zero pressure $G_0 = 121.960 \pm 0.087$ GPa and its pressure derivative $G' = 1.961 \pm 0.009$ for the NAL phase, and $G_0 = 129.653 \pm 0.059$ GPa and $G' = 2.340 \pm 0.004$ for the CF phase. The zero-pressure shear velocities of the NAL and CF phases are obtained to be 5.601 ± 0.005 km/sec and 5.741 ± 0.001 km/sec, respectively. We also found that shear velocity increases by 2.5 % upon phase transition from NAL to CF at around 40 GPa.

Keywords High pressure · NAL phase · CF phase · MORB · Sound velocity

L. Dai (✉)
Laboratory for High Temperature and High Pressure Study of the Earth's Interior, Institute of Geochemistry, Chinese Academy of Sciences, Guiyang 550002, Guizhou, China
e-mail: dailidong717@hotmail.com

L. Dai · Y. Kudo · K. Hirose · H. Ozawa
Department of Earth and Planetary Sciences, Tokyo Institute of Technology, 2-12-1 Ookayama, Meguro, Tokyo 152-8551, Japan

K. Hirose · H. Ozawa
Institute for Research on Earth Evolution, Japan Agency for Marine-Earth Science and Technology, 2-15 Natsushima, Yokosuka, Kanagawa 237-0061, Japan

M. Murakami · Y. Asahara
Department of Earth and Planetary Materials Science, Tohoku University, Sendai, Miyagi 980-8578, Japan

Y. Ohishi · N. Hirao
Japan Synchrotron Radiation Research Institute, 1-1-1 Kouto, Sayo, Hyogo 679-5198, Japan

Introduction

Previous high-pressure studies have reported that Al-rich phases constitute more than 20 % of the subducted mid-oceanic ridge basalt (MORB) crust in the lower mantle conditions (e.g., Irifune and Ringwood 1993; Kesson et al. 1994; Hirose et al. 1999, 2005; Ono et al. 2001; Ricolleau et al. 2008, 2010). Such Al-rich phases are the hexagonal new aluminum-rich (NAL) phase and the orthorhombic calcium ferrite (CF)-type phase. Both of these NAL and CF phases formed in a natural MORB bulk composition exhibit complex chemical formula (Guignot and Andrault 2004) but are approximately close in composition to $Na_{0.4}Mg_{0.6}Al_{1.6}Si_{0.4}O_4$ (40 % $NaAlSiO_4$–60 % $MgAl_2O_4$) (Imada et al. 2012). The earlier experiments on the join $NaAlSiO_4$-$MgAl_2O_4$ performed by Ono et al. (2009) and Imada et al. (2011) have revealed that the NAL phase with $Na_{0.4}Mg_{0.6}Al_{1.6}Si_{0.4}O_4$ composition undergoes transformation to the CF phase at around 40 GPa and 1,850 K with a density increase of about 2 %. More recently, by virtue of the first-principles computational method, Kawai and Tsuchiya (2012) found that the phase transition from NAL to CF occurs in $NaMg_2Al_5SiO_{12}$ (33 % $NaAlSiO_4$–67 % $MgAl_2O_4$) system at 40 GPa and 0 K, consistent with the experiments by Imada et al. (2011).

The change in elastic property across the phase transition from NAL to CF may contribute to the seismic heterogeneities in the mid-lower mantle. Theoretical work by Xu et al. (2008) provided the elastic parameters of the CF phase for both $NaAlSiO_4$ and $MgAl_2O_4$ end-members. Kawai and Tsuchiya (2012) calculated the elasticity of NAL and CF, demonstrating the changes in compressional wave velocity (−0.2 %) and shear wave velocity (+0.9 %). However, till now, the sound velocities of NAL and CF have not been measured.

In this work, we synthesized polycrystalline $Na_{0.4}Mg_{0.6}Al_{1.6}Si_{0.4}O_4$ NAL and CF at high pressure in a laser heating diamond anvil cell (DAC) and measured their shear velocities based on the Brillouin scattering spectroscopy method. The velocity measurements were conducted to 38 GPa for the NAL phase and to 73 GPa for the CF phase. On the basis of earlier compression study (Imada et al. 2012), shear modulus and its pressure derivative were obtained for both phases. In combination with the previously reported bulk moduli of NAL and CF, longitudinal velocities are also estimated.

Sample preparation and experimental details

A synthetic gel with the chemical composition of $Na_{0.4}Mg_{0.6}Al_{1.6}Si_{0.4}O_4$ was adopted to produce a reactive and homogenous starting material that is similar to be described by Ono et al. (2009). The gel was prepared in the department of earth and planetary sciences, Tokyo Institute of Technology as follows. High-purity chemical reagent Fe, MgO, $CaCO_3$, Na_2CO_3, and K_2CO_3 were dissolved into the dilute 5 wt % nitric acid, and then mixed together with solutions of $(C_2H_5O)_4Si$, $Al(NO_3)$, and ammonia. The gel was precipitated from the mixed solution and dried. The dried gel was ground and heated to 1,273 K for 15 min under controlled oxygen fugacity close to iron–wüstite buffer before high-pressure experiments. In order to prepare the synthetic NAL phase sample from dry gel, we enhanced the sample chamber pressure up to 30 GPa in a diamond anvil cell and then synthesized it under constant pressure and increasing the temperature up to 1,373 K for 3 min using the CO_2 laser heating system. The CF phase was similarly obtained by heating for 5 min at 50 GPa and 1,373 K. The details of annealing experiments are described by Kudo et al. (2012).

High pressure was generated by a symmetric DAC using anvil with 300 μm culet sizes. A pre-pressed gel sample and a NaCl pressure medium were loaded into a 100 μm hole in a rhenium gasket. The polycrystalline NAL and CF samples were synthesized in the DAC by heating with a CO_2 laser. Phase identification was made by synchrotron X-ray diffraction measurements at BL10XU in SPring-8. Angle-dispersive XRD spectra were collected on a CCD detector (Bruker APEX) and an imaging plate (IP, Rigaku). Exposure time was 10–40 s and 3–11 min for CCD and IP, respectively. A monochromatic incident X-ray beam with a wavelength of 0.41232–0.41435 Å was collimated to 15 μm in diameter. Two-dimensional XRD images were integrated as a function of two-theta angle in order to have conventional one-dimensional diffraction profiles using the Wt-2D program (Hammersley 1998). The representative X-ray diffraction spectra of the NAL and CF samples at high pressure are shown in Fig. 1. The NAL phase is characterized by its 110 peak around 3 degrees of two-theta angle. All the experimental pressures were determined after thermal annealing based on the Raman spectra of diamond (Akahama and Kawamura 2004). These pressures obtained from the Raman spectra were indeed consistent with those estimated from the unit cell volume of the B_1 or B_2 phase of NaCl in the sample center both before and after each experiment (Sata et al. 2002; Liu et al. 2010). The pressure difference between Raman spectra and B_2 phase of NaCl is less than 1.0 GPa. The equation of state obtained by Imada et al. (2012) was applied to conduct pressure calibration for the NAL and CF phases.

Brillouin scattering measurements were performed at SPring-8 (Murakami et al. 2009a, 2012). The sample was

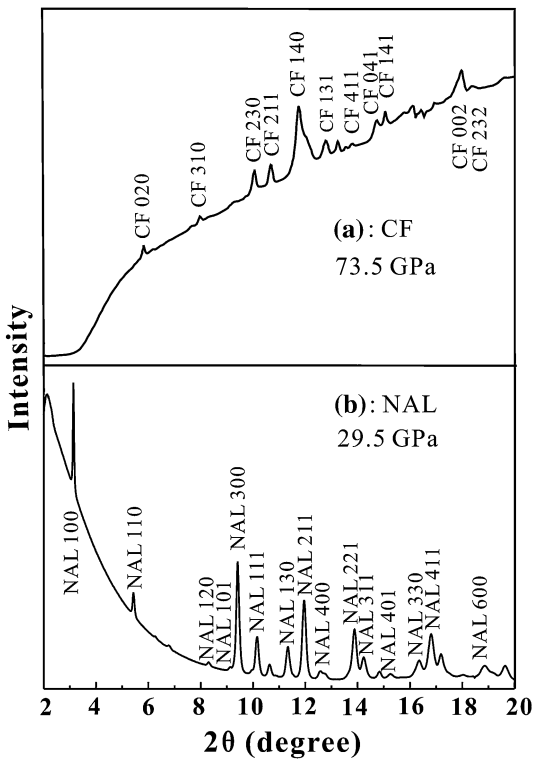

Fig. 1 Representative X-ray diffraction patterns of **a** CF at 73.9 GPa and **b** NAL at 29.3 GPa with the wavelength of 0.41332 and 0.41371 Å, respectively

annealed by heating with the CO_2 laser each time before the Brillouin scattering measurements, in order to reduce the stress state of the sample. The data collection time for a single spectrum varied from 4 to 24 h. The DAC was rotated with respect to the compression axis, and the shear velocity was measured at least five different chi angles at a given pressure condition. As described by Kawai and Tsuchiya (2012), the crystals of NAL and CF phases are hexagonal and orthorhombic, respectively. Along with the different crystallographic axis direction, the acoustic properties are anisotropic in most cases. By the average of different chi angles sound velocity, we can eliminate the anisotropic effect on the measurement results.

All measurements were performed in a platelet scattering geometry. In order to calibrate the scattering geometry, BK_7 borosilicate crown optical glass is used as a standard material (Yoneda and Song 2005). The external scattering angle was about 50°, which was calibrated by using a single-crystal MgO standard. In the platelet geometry, the sound velocity is determined from the Brillouin frequency shift of a given acoustic mode using the equation proposed by Whitfield et al. (1976):

$$V_i = \Delta\varpi_i \lambda / 2 \sin(\theta/2) \quad (1)$$

where V_i is the sound velocity of sample, $\Delta\omega_i$ is the frequency shift of Brillouin scattering spectra, λ is the wavelength of the incident laser (532 nm), θ is the angle of incidence between the laser beam and the outer surface of the diamond anvil, and i is one of the acoustic modes. For a detailed description of Brillouin scattering measurement system, see Murakami et al. (2009a, 2012) and Asahara et al. (2010a, b).

Results

All experimental results including shear velocities, shear moduli, and unit cell volumes of the NAL and CF phases at high pressures and room temperature conditions are summarized in Table 1. The aggregate shear velocities were determined in a pressure range from 9.4 to 38.4 GPa for the NAL phase and from 18.4 to 73.9 GPa for the CF phase. The representative Brillouin spectra are shown in Fig. 2. The longitudinal wave velocity could not be directly obtained from these spectra, because of the peak overlapping with the shear acoustic mode of diamond. Owing to a small thickness of NaCl pressure medium, its corresponding peak was also not observed.

As shown in Fig. 3, shear velocities of NAL phase were measured at room temperature in eight different directions as a function of chi angle with an increment of 0°, 45°, 90°, 135°, 180°, 215°, 270°, and 315° at 29.3 GPa. Other similar results on the anisotropic sound velocity check on the NAL and CF phases are also conducted under at least five different chi angles directions. Then, we make one average from each obtained different chi angles of sound velocity results at a given pressure condition, and thus greatly enhance the experimental precision of sound wave velocity measurement and efficiently reduce the anisotropic effect. The aggregate shear velocities of the NAL and CF phases measured at 300 K are shown as a function of pressure in Fig. 4. They are broadly consistent with previous theoretical results on $NaMg_2Al_5SiO_{12}$ (33 % $NaAlSiO_4$–67 % $MgAl_2O_4$) composition at 0 K as shown in Fig. 4 (Kawai and Tsuchiya 2012). However, our shear velocity data for NAL exhibit systematically lower velocity than those for CF at equivalent pressure. It results in the 2.5 % increase in shear velocity across the phase transition from NAL to CF at around 40 GPa. On the other hand, the calculations by Kawai and Tsuchiya (2012) found that the NAL and CF phases have comparable shear velocities, leading to <1 % velocity difference across the phase transition.

In order to estimate the shear modulus and its pressure derivative, the present pressure–shear velocity data were fitted to the third-order Eulerian finite strain equation, using the volume compression data reported by Imada et al. (2012):

$$\rho V_S^2 = G = G_0 (1+2f)^{\frac{5}{2}} \left\{ 1 - \left(5 - \frac{3K_{S0}G'}{G_0} \right) f \right\} \quad (2)$$

Table 1 Summary of shear velocities, shear moduli, and unit cell volumes for the NAL and CF phases at high pressures and room temperature conditions

Mineral phase	Pressure (GPa)[a]	V_s (km/s)	G (GPa)	Unit cell volume
NAL	9.4 (3)	5.860 (21)	139.81 (98)	174.690 (74)
	17.6 (6)	6.083 (13)	153.60 (72)	169.342 (66)
	29.3 (5)	6.292 (9)	173.42 (30)	163.063 (39)
	38.4 (8)	6.503 (15)	186.70 (78)	158.951 (46)
CF	18.4 (3)	6.243 (12)	166.84 (59)	33.204 (35)
	30.5 (4)	6.494 (27)	187.52 (131)	31.932 (54)
	50.9 (15)	6.821 (19)	217.51 (80)	30.313 (51)
	62.0 (11)	6.984 (12)	234.02 (57)	29.612 (46)
	73.9 (18)	7.142 (31)	249.81 (145)	28.960 (63)

[a] The equation of state obtained by Imada et al. (2012) was applied to conduct pressure calibration for the NAL and CF phases

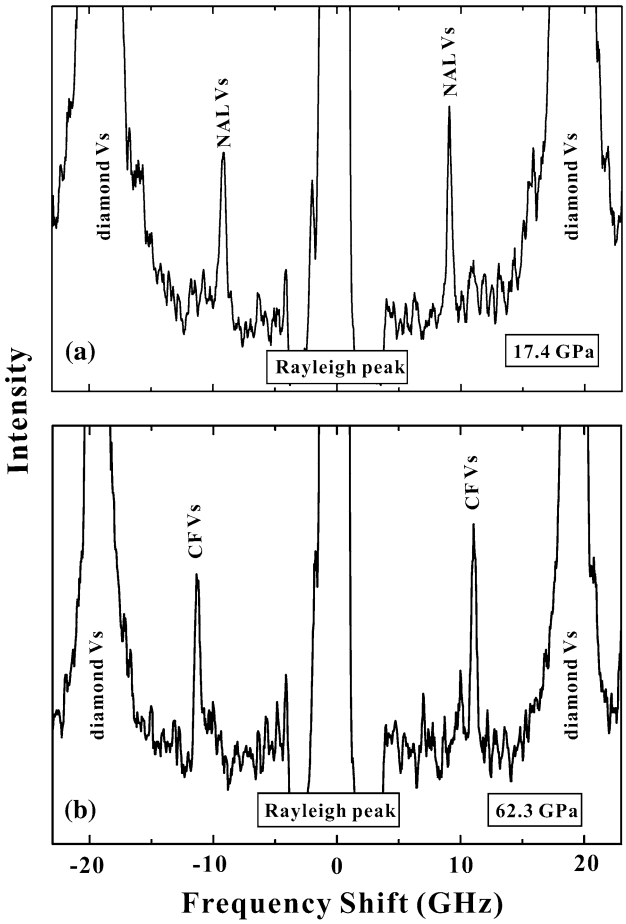

Fig. 2 Representative Brillouin scattering spectra of **a** NAL phase at 17.4 GPa and **b** CF phase at 62.3 GPa

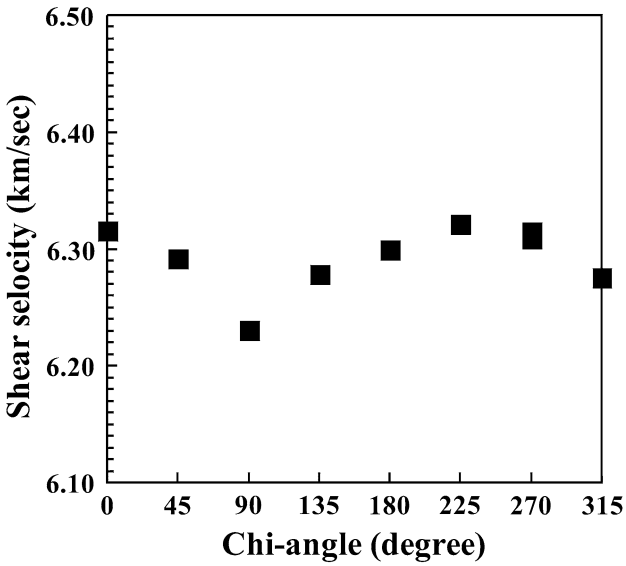

Fig. 3 Shear velocities of NAL phase under room temperature in eight different directions as a function of chi angle with an increment of 0°, 45°, 90°, 135°, 180°, 215°, 270°, and 315° at 29.3 GPa

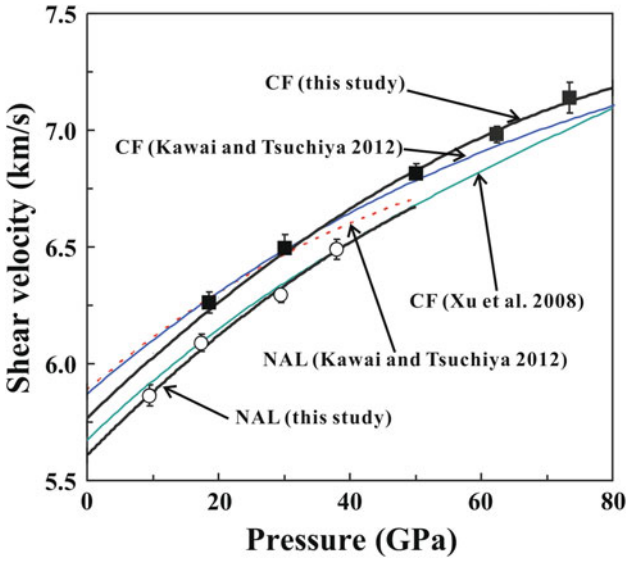

Fig. 4 Shear velocities of NAL and CF phases (*black solid lines*) obtained in this study compared with the previous theoretical calculation results. The *red broken line* and the *green* and *blue solid curves* represent NAL and CF phases from Kawai and Tsuchiya (2012), and as well as the CF phase from Xu et al. (2008), respectively

$$f = \frac{1}{2}\left\{\left(\frac{\rho}{\rho_0}\right)^{\frac{2}{3}} - 1\right\} \tag{3}$$

where ρ is the density at each given pressure, ρ_0 is the density at zero pressure, V_s is the shear velocity, G and G' are the adiabatic shear modulus and its pressure derivative, and K_{s0} is the adiabatic bulk modulus at zero pressure that we assume is equivalent to the isothermal bulk modulus (K_{T0}) at room pressure. The subscript zero denotes the value at ambient pressure. The fitting results give $G_0 = 121.960 \pm 0.087$ GPa and $G' = 1.961 \pm 0.009$ for the NAL phase, and $G_0 = 129.653 \pm 0.059$ GPa and $G' = 2.340 \pm 0.004$ for the CF phase. The change in shear modulus with increasing pressure is illustrated in Fig. 5. The shear modulus increases by 1.8 % across the phase transition from NAL to CF. With these shear modulus values and the bulk modulus and density data reported by Imada et al. (2012), the longitudinal wave velocities of the NAL and CF phases are also calculated (Table 2 and Fig. 6).

Implications for the lower mantle

Present results indicate the 2.5 % shear velocity increase upon phase transition from NAL to CF at around 40 GPa pressure condition (Fig. 4), corresponding to ~1,000 km depth, whereas the longitudinal velocity changes very little (<0.1 %) (Fig. 6). The volume compression study by

Imada et al. (2012) demonstrated that the density increases by 2.1 % across the NAL to CF phase transition. These may contribute to the seismic heterogeneity in the upper to middle part of the lower mantle, depending on the proportion of Al-rich phases and the sharpness of the transition between NAL and CF.

Both NAL and CF phases are the host of alkali elements in the lower mantle. They are known to be the major phases of the subducted MORB crust (e.g., Miyajima et al. 2001; Hirose and Fei 2002; Perrillat et al. 2006). The subducting continental crust (Yamamoto et al. 2009) and sedimentary rocks are enriched in such alkali elements and therefore possibly include large proportion of the NAL and CF phases in the lower mantle, although the phase relations of these materials have been determined only up to 24 GPa (Irifune and Ringwood 1994; Wu et al. 2009). The recent experimental study by Ricolleau et al. (2010) demonstrated that the NAL phase constitutes up to 20 % of the former MORB crust in the uppermost lower mantle conditions. In this case, ~0.5 % shear velocity and ~0.4 % density increases are expected to occur upon phase transition from NAL to CF with increasing pressure. Nevertheless, the sharpness of the NAL–CF transition strongly depends on the chemical composition. Imada et al. (2011) demonstrated that it occurs very sharply in 50 %$NaAlSiO_4$–50 %$MgAl_2O_4$ composition, while it takes place over ~10 GPa, corresponding to about 200 km depth range, in 40 %$NaAlSiO_4$–60 %$MgAl_2O_4$ composition. Ricolleau et al. (2010) also showed that the proportion of NAL phase diminished from 35 to 50 GPa in a natural MORB bulk composition, although small difference in sodium content likely changes the sharpness of the transition. If this is the case, the associated increases in shear velocity and density are smeared out in a wide depth range (~300 km), which would not be observed as anomaly in seismology.

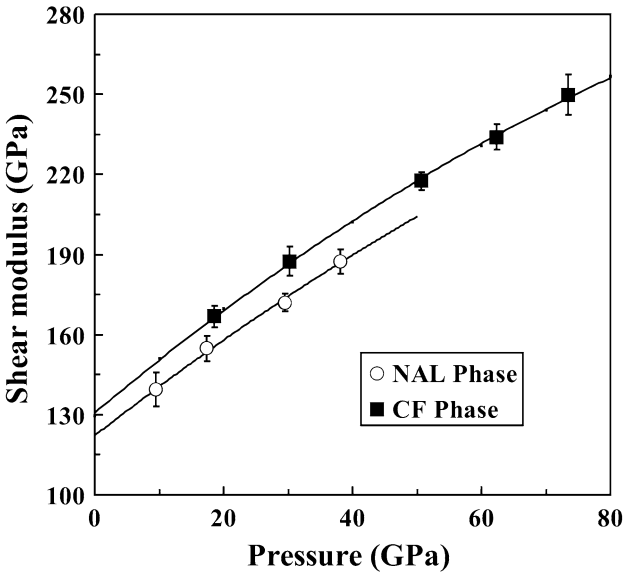

Fig. 5 Shear modulus of NAL and CF phases as a function of pressure at 300 K

We compare the shear velocities of NAL and CF with those of other typical lower mantle phases, determined experimentally at 300 K or theoretically at 0 K (Fig. 7). These Al-rich phases exhibit the lowest shear velocity among major lower mantle minerals, except tetragonal $CaSiO_3$ perovskite (Kudo et al. 2012). On the other hand, the longitudinal velocities of NAL and CF are lower than those of pure $MgSiO_3$ perovskite and SiO_2 phase, but higher than those of MgO and tetragonal $CaSiO_3$ perovskite (Fig. 8).

As argued by Xu et al. (2008), the low shear velocity of CF is well compensated for by high velocity of SiO_2 phase, leading to higher shear velocity of subducted MORB crust than that of pyrolytic lower mantle. According to the results by Karki et al. (1997), the shear wave velocity of SiO_2 decreases rapidly up to ~60 % at around 45 GPa due to the phase transition from stishovite to the $CaCl_2$ structure phase. As mentioned earlier, subducted continental crust and sediments likely include substantial amount of

Table 2 Comparison of elastic properties of NAL and CF phases

Source	Chemical composition	G_0 (GPa)	G'	V_{s0} (km/s)	V_{p0} (km/s)	Max P (GPa)	Remarks (K)
Experiments							
In this study	NAL phase $Na_{0.4}Mg_{0.6}Al_{1.6}Si_{0.4}O_4$	121.960 (87)	1.961 (9)	5.601 (5)	9.643 (9)[a]	38.4	300
	CF phase $Na_{0.4}Mg_{0.6}Al_{1.6}Si_{0.4}O_4$	129.653 (59)	2.340 (4)	5.741 (1)	9.321 (2)	73.9	300
Theory							
Xu et al. (2008)	CF phase $Na_{0.4}Mg_{0.6}Al_{1.6}Si_{0.4}O_4$	132.721 (3)	1.953 (8)	5.812 (7)	9.642 (4)	80	1,600
Kawai and Tsuchiya (2012)	NAL phase $Na_{0.33}Mg_{0.67}Al_{1.67}Si_{0.33}O_4$	125.570 (13)	1.854 (2)	5.624 (3)	9.842 (7)	80	0
Kawai and Tsuchiya (2012)	CF phase $Na_{0.33}Mg_{0.67}Al_{1.67}Si_{0.33}O_4$	137.072 (98)	1.830 (5)	5.830 (1)	9.910 (0)	80	0

Numbers in the parentheses are standard deviations in the last digit(s)

[a] Only the uncertainty in shear modulus is considered for error estimation

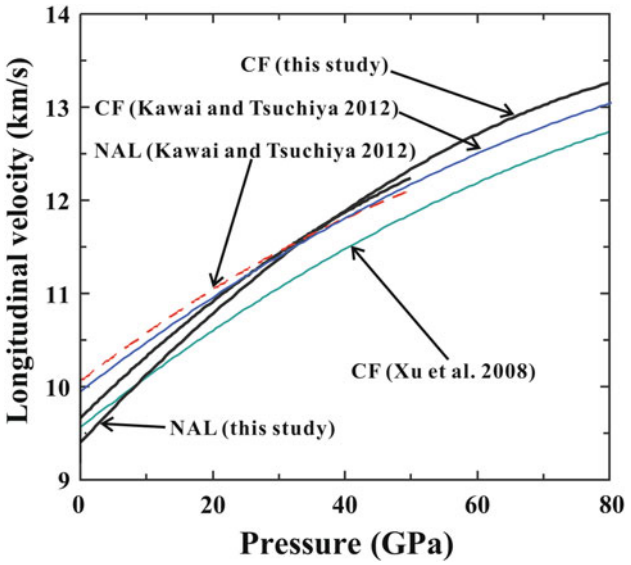

Fig. 6 Shear velocities of NAL and CF phases (*black solid lines*) obtained in this study compared with the previous theoretical calculation results. The *red broken line* and the *green* and *blue solid curves* represent NAL and CF phases from Kawai and Tsuchiya (2012), and as well as the CF phase from Xu et al. (2008), respectively

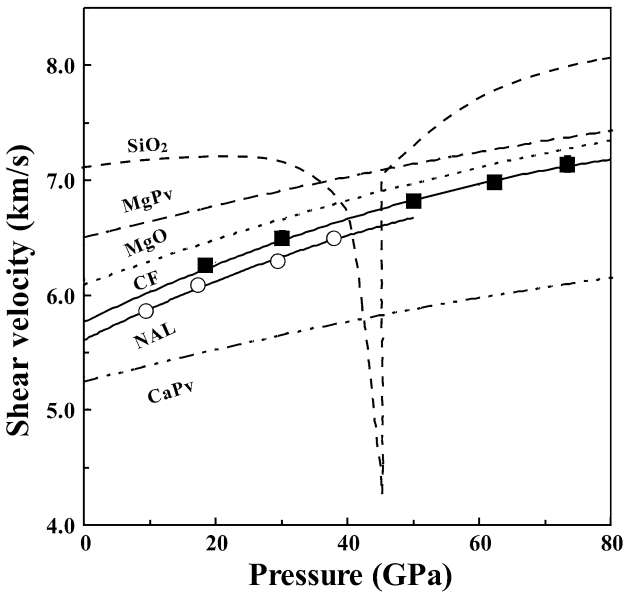

Fig. 7 Measured (300 K) or calculated (0 K) shear velocities of typical lower mantle minerals at high pressures shown in solid lines of this study. The *dashed lines* are from Ca-perovskite (Kudo et al. 2012), MgO (Murakami et al. 2009b), $MgSiO_3$ perovskite (Murakami et al. 2007), and SiO_2 phase (Karki et al. 1997), respectively. As pointed by Karki et al. (1997), the shear wave velocity of SiO_2 decreases rapidly up to ~60 % at around 45 GPa due to the phase transition from stishovite to the $CaCl_2$ structure phase

NAL or CF phases as well, but are more enriched in the SiO_2 phase, which would result in considerably higher velocity as a bulk system.

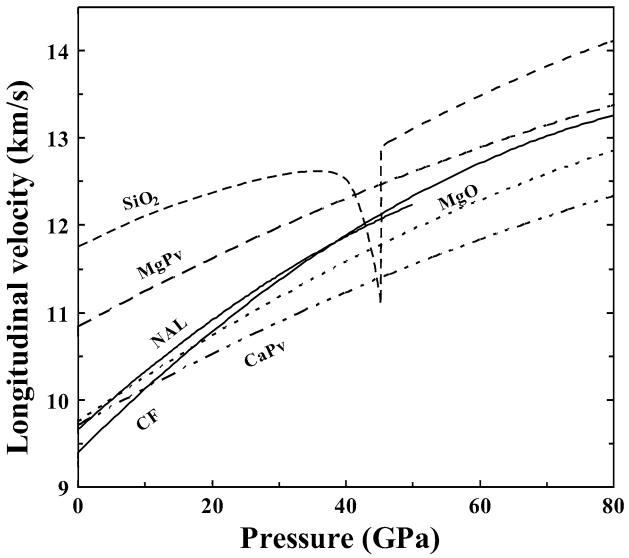

Fig. 8 The calculated longitudinal velocities of typical lower mantle minerals at high pressures and temperature of 0 or 300 K shown in *solid lines* of this study. The *dashed lines* are from Ca-perovskite (Kudo et al. 2012), MgO (Murakami et al. 2009b), $MgSiO_3$ perovskite (Murakami et al. 2007), and SiO_2 phase (Karki et al. 1997), respectively. As pointed by Karki et al. (1997), the shear wave velocity of SiO_2 decreases rapidly up to ~60 % at around 45 GPa due to the phase transition from stishovite to the $CaCl_2$ structure phase

It has been suggested that the crystallization of $MgSiO_3$-rich perovskite from basal magma ocean evolves the composition of residual magma to be poor in SiO_2 and rich in MgO, FeO, and other incompatible elements such as Na_2O and K_2O (Labrosse et al. 2007; Nomura et al. 2011). Such residual melts are denser than any of the typical lower mantle minerals below 1,800 km depth and therefore may have accumulated at the base of the mantle. As a consequence, the late stage of crystallization from the basal magma ocean could have formed chemically anomalous solid patches being enriched in the (Mg, Fe)O ferropericlase and the CF phase in the lowermost mantle. As shown in Figs. 7 and 8, both ferropericlase and CF exhibit substantially lower sound velocities than those of $MgSiO_3$-rich perovskite (see Xu et al. 2008 and Murakami et al. 2012 for the effects of chemical impurity and high temperature). The enrichment in ferropericlase and the CF phase therefore causes large seismic anomaly, in particular remarkably low shear velocity, in the deep lower mantle. Note, however, that present measurements were performed on a simplified system, which may limit the direct application to the Earth's lower mantle.

Acknowledgments We thank two anonymous reviewers and editor of Professor Masanori Matsui for their very constructive comments and suggestions in the reviewing process, which helped us greatly in improving the manuscript. The enlightening discussions were conducted with Professor Heping Li and Dr Shuangming Shan from

Laboratory for High Temperature and High Pressure Study of the Earth's Interior, Institute of Geochemistry, CAS. Dr Saori Imada provides the starting material. The X-ray diffraction measurements were conducted at BL10XU, SPring-8 (Proposal no. 2011B0087 and 2012A0087). This research was financially supported by the "135" Program of Institute of Geochemistry, CAS, the Knowledge-Innovation Key Orientation Project of CAS (KZCX2-YWQN110), NSF of China (41174079 and 40974051), and the Japan Society for the Promotion of Science.

References

Akahama Y, Kawamura H (2004) High-pressure Raman spectroscopy of diamond anvils to 250 GPa: method for pressure determination in the multimegabar pressure range. J Appl Phys 96: 3748–3751

Asahara Y, Murakami M, Ohishi Y, Hirao N, Hirose K (2010a) Sound velocity measurement in liquid water up to 25 GPa and 900 K: implications for densities of water at lower mantle conditions. Earth Planet Sci Lett 289:479–485

Asahara Y, Hirose K, Ohishi Y, Hirao N, Murakami M (2010b) Thermoelastic properties of ice VII and its high-pressure polymorphs: implications for dynamics of cold slab subduction in the lower mantle. Earth Planet Sci Lett 299:474–482

Guignot N, Andrault D (2004) Equations of state of Na-K-Al host phase and implications for MORB density in the lower mantle. Phys Earth Planet Inter 143–144:107–128

Hammersley AP (1998) Fit2d: V9.129 reference manual v3.1. Inter Rep ESRF98HA01, ESRF, Grenoble

Hirose K, Fei YW (2002) Subsolidus and melting phase relations of basaltic composition in the uppermost lower mantle. Geochim Cosmochim Acta 66:2099–2108

Hirose K, Fei Y, Ma Y, Mao HK (1999) The fate of subducted basaltic crust in the Earth's lower mantle. Nature 397:53–56

Hirose K, Takafuji N, Sata N, Ohishi Y (2005) Phase transition and density of subducted MORB crust in the lower mantle. Earth Planet Sci Lett 237:239–251

Imada S, Hirose K, Ohishi Y (2011) Stabilities of NAL and Ca-ferrite-type phases on the join $NaAlSiO_4$-$MgAl_2O_4$ at high pressure. Phys Chem Minerals 8:557–560

Imada S, Hirose K, Komabayashi T, Suzuki T, Ohishi Y (2012) Compression of $Na_{0.4}Mg_{0.6}Al_{1.6}Si_{0.4}O_4$ NAL and Ca-ferrite-type phases. Phys Chem Minerals 39:525–530

Irifune T, Ringwood AE (1993) Phase transformations in subducted oceanic crust and buoyancy relationships depths of 600–800 km in the mantle. Earth Planet Sci Lett 117:101–110

Irifune T, Ringwood AE (1994) Subduction of continental crust and terrigenous and pelagic sediments: an experimental study. Earth Planet Sci Lett 126:351–368

Karki B, Stixrude L, Crain J (1997) Ab initio elasticity of three high-pressure polymorphs of silica. Geophys Res Lett 24:3269–3272

Kawai K, Tsuchiya T (2012) Phase stability and elastic properties of the NAL and CF phases in the $NaMg_2Al_5SiO_{12}$ system from first principles. Am Mineral 97:305–314

Kesson SE, Fitz GJD, Shelley JMG (1994) Mineral chemistry and density of subducted basaltic crust at lower-mantle pressures. Nature 372:767–769

Kudo Y, Hirose K, Murakami M, Asahara Y, Ozawa H, Ohishi Y, Hirao N (2012) Sound velocity measurements of $CaSiO_3$ perovskite to 133 GPa and implications for lowermost mantle seismic anomalies. Earth Planet Sci Lett 349–350:1–7

Labrosse S, Hernlund JW, Coltice N (2007) A crystallizing dense magma ocean at the base of Earth's mantle. Nature 450:866–869

Liu L, Bi Y, Xu J, Chen XR (2010) Ab initio study of the elastic properties of sodium chloride at high pressure. Phys B 405:2175–2180

Miyajima N, Yagi T, Hirose K, Kondo T, Fujino K, Miura H (2001) Potential host phase of aluminum and potassium of the Earth's lower mantle. Am Mineral 86:740–746

Murakami M, Sinogeikin SV, Hellwig H, Bass JD, Li J (2007) Sound velocity of $MgSiO_3$ perovskite to Mbar pressure. Earth Planet Sci Lett 256:47–56

Murakami M, Asahara Y, Ohishi Y, Hirao N, Hirose K (2009a) Development of in situ Brillouin spectroscopy at high pressure and temperature with synchrotron radiation and infrared laser heating system: application to the Earth's deep interior. Phys Earth Planet Inter 174:282–291

Murakami M, Ohishi Y, Hirao N, Hirose K (2009b) Elasticity of MgO to 130 GPa: implications for lower mantle mineralogy. Earth Planet Sci Lett 277:123–129

Murakami M, Ohishi Y, Hirao N, Hirose K (2012) A perovskite lower mantle inferred from high-pressure, high-temperature sound velocity data. Nature 485:90–94

Nomura R, Ozawa H, Tateno S, Hirose K, Hernlund J, Muto S, Ishii H, Hiraoka N (2011) Spin crossover and iron-rich silicate melt in the Earth's deep mantle. Nature 473:199–202

Ono S, Ito E, Katsura T (2001) Mineralogy of subducted basaltic crust (MORB) from 25 to 37 GPa, and chemical heterogeneity of the lower mantle. Earth Planet Sci Lett 90:57–63

Ono A, Akaogi M, Kojitani H, Yamashita K, Kobayashi M (2009) High-pressure phase relations and thermodynamic properties of hexagonal aluminous phase and calcium-ferrite phase in the systems $NaAlSiO_4$-$MgAl_2O_4$ and $CaAl_2O_4$-$MgAl_2O_4$. Phys Earth Planet Inter 174:39–49

Perrillat JP, Ricolleau A, Daniel I, Fiquet G, Mezouar M, Guignot N, Cardon H (2006) Phase transformations of subducted basaltic crust in the upmost lower mantle. Phys Earth Planet Inter 157:139–149

Ricolleau A, Fiquet G, Addad A, Menguy N, Vanni C, Perrillat JP, Daniel I, Cardon H, Guignot N (2008) Analytical transmission electron microscopy study of a natural MORB sample assemblage transformed at high pressure and high temperature. Am Mineral 93:144–153

Ricolleau A, Perrillat JP, Fiquet G, Daniel I, Matas J, Addad A, Menguy N, Cardon H, Mezouar M, Guignot N (2010) Phase relations and equation of state of a natural MORB: implications for the density profile of subducted oceanic crust in the Earth's lower mantle. J Geophys Res 115:B08202. doi:10.1029/2009JB006709

Sata N, Shen G, Rivers ML, Sutton SR (2002) Pressure-volume equation of state of the high-pressure B_2 phase of NaCl. Phys Rev B 65:104114. doi:10.1103/PhysRevB.65.104114

Whitfield CH, Brody EM, Bassett WA (1976) Elastic moduli of NaCl by Brillouin scattering at high pressure in a diamond cell. Rev Sci Instrum 47:942–947

Wu Y, Fei YW, Jin ZM, Liu XY (2009) The fate of subducted upper continental crust: an experimental study. Earth Planet Sci Lett 282:275–284

Xu W, Lithgow-Bertelloni C, Stixrude L, Ritsema J (2008) The effect of bulk composition and temperature on mantle seismic structure. Earth Planet Sci Lett 275:70–79

Yamamoto S, Nakajima J, Hasegawa A, Maruyama S (2009) Izu-Bonin arc subduction under the Honshu island, Japan: evidence from geological and seismological aspect. Gondwana Res 16:572–580

Yoneda A, Song MS (2005) Frequency domain analysis of ultrasonic velocity: an alternative bond effect correction constraining bond properties. J Appl Phys 97:024908. doi:10.1063/1.1834711